Structural relaxation and nanoindentation response in Zr–Cu–Ti amorphous thin films

H. S. Chou,[1] J. C. Huang,[1,a)] L. W. Chang,[1] and T. G. Nieh[2]
[1]*Department of Materials and Optoelectronic Science, Center for Nanoscience and Nanotechnology, National Sun Yat-Sen University, Kaohsiung 804, Taiwan*
[2]*Department of Materials Science and Engineering, University of Tennessee, Knoxville, Tennessee 37996, USA*

(Received 8 August 2008; accepted 19 September 2008; published online 10 November 2008)

Ternary Zr–Cu–Ti system, especial with a high Ti content, is normally difficult to be fully vitrified. In this paper, we demonstrate that cosputtering can produce amorphous Zr–Cu–Ti thin films with an excessive Ti content even as high as 19%. Sub-T_g annealing of the film induces the formation of medium-range-ordered clusters and to raise the nanohardness by 35% to 6.6 GPa. The promising mechanical properties of the sub-T_g annealed $Zr_{52}Cu_{29}Ti_{19}$ films offer great potential for microelectromechanical system applications. © *2008 American Institute of Physics*.
[DOI: 10.1063/1.2999592]

Amorphous alloys are considered promising for making the microelectromechanical systems (MEMS). For such applications, an amorphous alloy synthesized via sputtering process can provide a wide compositional window for the glass forming ability without microsegregation.[1] For example, Zhang *et al.*[2] have conducted bending test with notched, freestanding microbeam fabricated from Pd-based thin film metallic glasses by focus ion beam. Fukushige *et al.*[3] have utilized the superplastic forming ability of amorphous alloys in the supercooled liquid region to produce microactuators.

The most well known binary amorphous system is probably Cu–Zr, which can be prepared by cosputtering[4] or multilayer sputtering plus postannealing.[5–7] However, the hardness (~3.5–4.0 GPa) and modulus (~80–100 GPa) of Cu–Zr binary thin films are relatively low for a typical MEMS device. One solution is to add Ti to improve the hardness and modulus values over 5 and 120 GPa, respectively, such that the MEMS device can have sufficient strength, torque, and wear resistance. For the ternary Cu–Zr–Ti amorphous system, most studies have been focused on the Cu-rich bulk metallic glasses.[8,9] Although the heat of mixing (ΔH_{mix}) for Zr–Ti is nearly ~0 kJ/mol, thermal resistance of the Ti-containing Cu–Zr–Ti alloys was found to be better than that of the Ti-free alloys.[8,10]

There have been several studies on the cast or roll-bonded binary Zr–Cu, Zr–Ti, and ternary Zr–Cu–Ti amorphous alloys.[10–12] However, there was no report on the study of cosputtered thin films. In bulk form, the glass forming ability and supercooled temperature region of Cu–Zr is significantly degraded by adding excessive Ti.[10] It is, therefore, highly unlikely to produce a fully amorphous bulk specimen with the Ti content more than 10 at. %. Having a much faster quenching rate, thin film metallic glasses (THMGs) can offer a much wider composition and processing window. Consequently, a composition of $Zr_{52}Cu_{29}Ti_{19}$ with an excessive Ti content is selected for this study.

The response of the amorphous alloys below the glass transition temperature T_g is of interest because sub-T_g is usually the actual application temperature. For example, the metallic thin films for MEMS or semiconductors might be exposed during photolithography soft baking or hard baking at temperatures below T_g. Sub-T_g annealing would induce structural relaxation in various forms.[13] For example, Murali and Ramamurty[14] have conducted the sub-T_g annealing to study the change of mechanical properties between the as-cast and annealed $Zr_{41.2}Ti_{13.75}Cu_{12.5}Ni_{10}Be_{22.5}$. Daniel *et al.*[15] also performed the creep of a Zr–Cu–Al–Ni bulk glass annealed near T_g to study the effect of structural relaxation on the creep behavior. No systematic study has been conducted on the sub-T_g response of THMGs.

The $Zr_{52}Cu_{29}Ti_{19}$ thin films were codeposited on silicon substrates using the magnetron cosputtering. The thickness of the as-deposited films is 2.2 μm. It was not possible to conduct differential scanning calorimetry measurement for the film itself since it is difficult to safely detach the thin film from the substrate. We adopt the published values of glass transition and crystallization temperatures T_g and T_x, which are estimated to be around 625 and 645 K,[10] respectively. The as-deposited specimens, denoted as specimens A, were annealed at 473 and 563 K for 1 h in a vacuum environment, denoted as specimens B and C. These specimens were subsequently characterized by x-ray diffraction (XRD), transmission electron microscopy (TEM), and field-emission high resolution TEM (HRTEM). The compositions were measured by the energy-dispersive spectrometry in scanning electron microscopy. The TEM specimens were prepared by ion milling below 3 keV in order to minimize possible crystallization during the milling. The as-deposited and annealed specimens were indented using a MTS XP nanoindentation system at room temperature at a loading rate of 0.01 mN/s, up to the maximum load of 5 mN. The oxygen contents were measured by the Auger electron spectroscopy (AES).

The XRD pattern from the as-deposited $Zr_{52}Cu_{29}Ti_{19}$ thin film exhibits the typical broad peak, indicating an amorphous structure. After annealing at 473 K (~$0.8T_g$) and 563 K (~$0.9T_g$) for 1 h, the film still remains amorphous, according to the XRD spectra. The peak widths at the half intensity Δ, indicative of the interatomic distance, are measured and the data are plotted in Fig. 1(a). With decreasing Δ

a)Author to whom correspondence should be addressed. Tel.: +886-7-525-2000 ext. 4063. Electronic mail: jacobc@mail.nsysu.edu.tw.

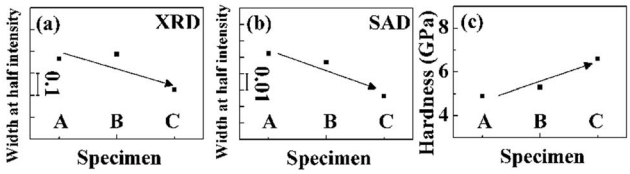

FIG. 1. The peak widths at the half intensity calculated from the (a) XRD and (b) TEM results, utilizing the peak fitting with the amplitude version of Gaussian peak function. The variation of hardness with the microstructural change is shown in (c).

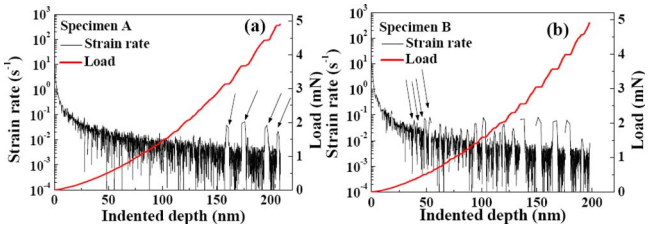

FIG. 3. (Color online) Relation between the strain rate and load versus indentation displacement for (a) specimen A and (b) specimen B. The curves for specimen C are similar to specimen B.

value, the interatomic distance appears to slightly reduce as a result of the sub-T_g annealing.

Figure 2(a) is the bright-field image of the as-deposited specimen A. The inserted selected area diffraction (SAD) pattern supporting the amorphous nature. After annealing at 473 and 563 K for 1 h, the amorphous nature still remains, as shown in Figs. 2(b) and 2(c). The intensity profiles of the SADs for the three specimens are also tracked electronically. The hump widths at the half intensity Δ' for the SADs are measured and plotted in Fig. 1(b). Again, the Δ' values show a decreasing trend upon annealing.

The load-depth curves obtained from nanoindentation are shown in Fig. 3. With the maximum load of 5 mN, the indented depths for specimens A, B, and C are 210, 203, and 190 nm, all lower than $\frac{1}{10}$ of the film thickness (2.2 μm) to minimize the substrate effect. The extracted hardness data are listed in Table I and also plotted in Fig. 1(c). The hardness is noted to increase from 4.9 GPa for the as-sputtered specimen A to 6.6 GPa for specimen C, or an appreciable increment of about 35%. These hardness values are noted to be much higher than that of binary Cu–Zr (3.5–4.0 GPa). Also listed in Table I are the modulus (E) value, which change only slightly from 120 to 125 GPa as a result of the sub-T_g annealing (or only 4% increment), indicating that the basic atomic bonding does not change much. The indentation pop-in phenomenon, generally attributed to shear band initiation, appears at a relatively late stage in the as-sputtered film, but shows a higher occurrence in the annealed films; this will be discussed later.

According to the XRD and TEM results, the basic amorphous nature still remains after the sub-T_g annealing, but the hardness increases by 35%. Three possible factors may contribute to the hardening and they are (1) oxygen effect, (2) formation of medium-range-ordering (MRO) clusters, and (3) annihilation of the atomic size holes.

Both Ti and Zr have a high oxygen affinity, thus oxygen pick-up during vacuum annealing must be considered. AES measurements from the three samples were done. It is found that the oxygen content in the as-deposited film A is limited to a thickness of about 8 nm from the surface. Oxygen profile for specimen B is similar to that for specimen A, suggesting that oxygen absorption at 473 K is insignificant. By contrast, the curve for specimen C, which was annealed at 563 K for 1 h, shows some oxygen pick up. However, oxygen absorption is still limited within 12 nm from the film surface. These surface layers are not expected to significantly affect the hardness values, which were obtained from an indentation depth of ~200 nm. Therefore, the oxygen absorption should not play a major role in the hardness increase.

Sub-T_g structure relaxation can proceed by various routes. During the relaxation, although long-range diffusion is not likely to occur, the thermal energy is sufficient to rearrange atoms locally (~1–2 nm) and form more stable MRO structures.[16,17] Structural examinations using TEM and HRTEM do not reveal the presence of crystalline phase greater than 2 nm. For example, Fig. 4(a) is a HRTEM image of specimen A. The encircled area exhibits a scattering pattern which is different from its surrounding region, suggesting the presence of MRO structure. The corresponding Fourier transformed diffraction patterns from the MRO region (taken with a square selected area of 1 nm^2) still show faint and diffuse contrast, indicating it is not a crystalline phase. It is noted, however, the density of MRO structure in the as-sputtered specimen A is relatively low. The population of MRO increases in specimens B [Fig. 4(b)] and C [Fig. 4(c)]. The population of MRO clusters in specimen C is higher than those in B and A. The presence of these MRO clusters in a glass matrix is expected to increase the resistance for shear band propagation, thereby the strength or hardness. This is similar to the case of having nanocrystals in a glass matrix.[18] A higher sub-T_g annealing temperature or longer annealing time is expected to produce more MRO clusters and, therefore, a higher hardness.

From a free-volume theory,[19] the strain rate is a function of he average free volume of an atom ν_f and the applied stress, σ. When the strain rate (or indentation rate) is fixed and at room or low temperature, the relation can be simplified as

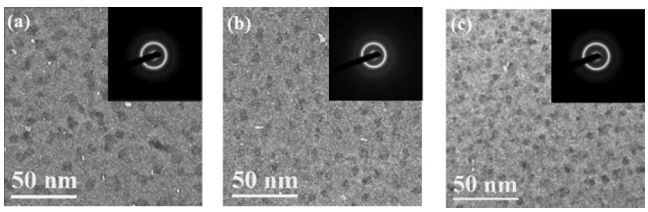

FIG. 2. TEM bright field micrographs of (a) the as-sputtered thin film, specimen A, (b) the film after annealing at 473 K, specimen B, and (c) the film after annealing at 563 K, specimen C. The spotty contrast is a result of ion milling, it is not from the crystalline phase.

TABLE I. The nanoindentation properties of specimens A, B, and C, tested at 0.01 mN/s. The data obtained from the binary Zr–Cu thin films in our laboratory are also included.

Specimen	Indentation depth h (nm)	Modulus E (GPa)	Hardness H (GPa)
$Zr_{50-70}Cu_{30-50}$ films	200	80–100	3.5–4.0
A	210	120 ± 5.90	4.9 ± 0.51
B	203	122 ± 7.12	5.3 ± 0.74
C	190	125 ± 7.55	6.6 ± 0.72

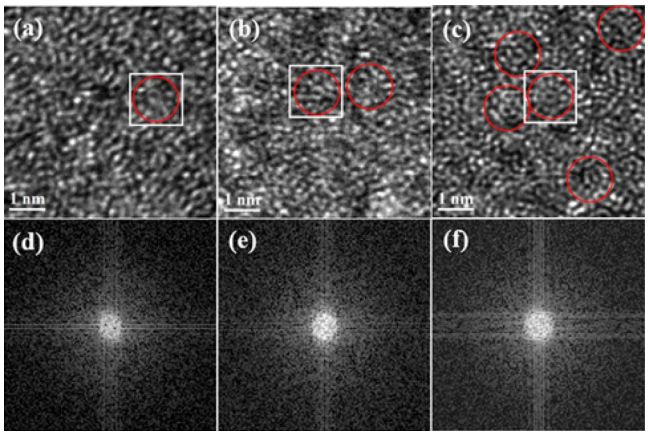

FIG. 4. (Color online) The high-resolution TEM image of (a) specimen A, (b) specimen B, and (c) specimen C. The marked circles correspond to the MRO clusters. (d), (e), and (f) show the Fourier transformed diffraction patterns for the white squares in (a), (b) and (c), respectively.

$$\sigma = \frac{2kT}{\varepsilon_0 v_0}\left(2\beta + \frac{\gamma v^*}{v_f}\right), \tag{1}$$

where k is the Boltzmann constant, T is the temperature, ε_0 is the strain of a flow unit, ν_0 is the volume of a flow unit, β is a constant, γ is a geometrical factor, ν^* is the effective hard-sphere size of the atom, and ν_f is the average free volume of an atom. Assume further that shear band formation is proportional to the average free volume density ν_f, it is evident that the strength of the material increases with a decreasing ν_f. In other words, the observed hardness increase after structural relaxation is a result of the reduction of free volume caused by sub-T_g annealing.

The amount and distribution of free volume obviously play the major role in the formation of shear bands.[19] Amorphous alloys synthesized via sputtering usually contain significant amount of atomic size defects.[13] In as-cast metallic glasses, open-volume defects could be broken into two categories: intrinsic voids surrounded by nine or less atoms and larger holes surrounded by ten or more atoms.[20–22] The intrinsic voids which are typically smaller than an atom exhibited certain similarity with Bernal's canonical holes. These voids cannot be removed by thermal annealing. By contrast, the larger holes with size approximately equal to an atom or termed as the atomic size holds were mainly nonspherical with some resemblance to crystalline vacancies. They can be removed by annealing.

During the nanoindentation of the as-deposited film (sample A), the atomic size holes serve as the sites for stress release during the initial stage of deformation. This results in a softer material and the delay of the onset of shear band formation, i.e., pop-in [Fig. 3(a)]. It was pointed out by Schuh *et al.*[23] that shear band would not nucleate unless shear transition zone (STZ) cluster has reached the critical size. This requires multiple STZs operating in a sequential fashion, assisted by the deformation-induced free volume. Thus, the onset of pop-in does not occur until the exhaustion of the atomic size holes and the creation of sufficient amount of deformation-induced free volume.

During sub-T_g annealing, atoms can rearrange locally without long-range diffusion, which reduces the average distance among atoms. The majority of atomic size holes were gradually annealed out and the structures in samples B and C are partially relaxed. Upon indentation, because of the lack of the atomic size holes to absorb deformation strain, pop-ins occur much earlier in these samples, as shown by arrows in Fig. 3(b) for specimen B. Similar situation occurs for specimen C.

In summary, a fully amorphous $Zr_{52}Cu_{29}Ti_{19}$ thin film can be prepared by cosputtering. With the high 19 at. % Ti added in the Zr–Cu film, the hardness and modulus can increase to 4.9 and 120 GPa, respectively, well above the levels of ~4 and ~90 GPa for the binary Zr–Cu amorphous films. Sub-T_g annealing at 0.8 and 0.9T_g further increases the film nanohardness to a level up to 6.6 GPa, or an increment of 35% and 89% as compared to the as-sputtered $Zr_{52}Cu_{29}Ti_{19}$ film (4.9 GPa) and binary Zr–Cu films (~4 GPa), respectively. The pronounced increment in strength offers great opportunity for making a stronger MEMS device. Based on the HRTEM and pop-in analyses, it is reasonable to conclude that the pronounced increase of nano-hardness is attributed to the formation of MRO clusters (~1 nm in size) and the vanish of the free volumes and atomic size holes during sub-T_g annealing.

The authors acknowledge the sponsorship from Nation Science Council of Taiwan, ROC, under the Grant No. NSC 95-2221-E-110-013-MY3. T.G.N. was supported by the US Department of Energy, Office of Basic Energy Sciences, under contract DE-FG02-06ER46338 with the University of Tennessee.

[1] J. P. Chu, C. T. Liu, T. Mahalingam, S. F. Wang, M. J. O'Keefe, B. Johnson, and C. H. Kuo, Phys. Rev. B **69**, 113410 (2004).
[2] G. P. Zhang, Y. Liu, and B. Zhang, Scr. Mater. **54**, 897 (2006).
[3] T. Fukushige, S. Hata, and A. Shimokohbe, J. Microelectromech. Syst. **14**, 243 (2005).
[4] J. Dudonis, R. Brucas, and A. Miniotas, Thin Solid Films **275**, 164 (1996).
[5] T. G. Nieh and J. Wadsworth, Scr. Mater. **44**, 1825 (2001).
[6] T. G. Nieh, T. W. Barbee, and J. Wadsworth, Scr. Mater. **41**, 929 (1999).
[7] Q. Wang, J. B. Qiang, J. H. Xia, J. Wu, Y. M. Wang, and C. Dong, Intermetallics **15**, 711 (2007).
[8] H. Man, J. Y. Fu, C. L. Ma, S. J. Pang, and T. Zhang, J. Univ. Sci. Technol. Beijing **14**, 19 (2007).
[9] A. Inoue, W. Zhang, T. Zhang, and K. Kurosaka, Acta Mater. **49**, 2645 (2001).
[10] Y. T. Shen, L. Q. Xing, and K. F. Kelton, Philos. Mag. **85**, 3673 (2005).
[11] P. J. Hsieh, Y. P. Hung, and J. C. Huang, Scr. Mater. **49**, 173 (2003).
[12] G. P. Dinda, H. Rosner, and G. Wilde, J. Non-Cryst. Solids **353**, 3777 (2007).
[13] A. R. Yavari, A. L. Moulec, A. Inoue, N. Nishiyama, N. Lupu, E. Matsubara, W. J. Botta, G. Vaughan, M. D. Michel, and A. Kvick, Acta Mater. **53**, 1611 (2005).
[14] P. Murali and U. Ramamurty, Acta Mater. **53**, 1467 (2005).
[15] B. S. S. Daniel, A. R. Leonhard, M. Heilmaier, J. Eckert, and L. Schultz, Mech. Time-Depend. Mater. **6**, 193 (2002).
[16] X. J. Liu, G. L. Chen, H. Y. Hou, X. Hui, K. F. Yao, Z. P. Liu, and C. T. Liu, Acta Mater. **56**, 2760 (2008).
[17] Y. Hirotsu, T. G. Nieh, A. Hirata, T. Ohkubo, and N. Tanaka, Phys. Rev. B **73**, 012205 (2006).
[18] A. Inoue, H. M. Kimura, and T. Zhang, Mater. Sci. Eng., A **294**, 727 (2000).
[19] F. Spaepen, Acta Metall. **25**, 407 (1977).
[20] J. Sietsma and B. J. Thijsse, Phys. Rev. B **52**, 3248 (1995).
[21] D. B. Miracle, T. Egami, K. M. Flores, and K. F. Kelton, MRS Bull. **32**, 629 (2007).
[22] K. M. Flores, E. Sherer, A. Bharathula, H. Chen, and Y. C. Jean, Acta Mater. **55**, 3404 (2007).
[23] C. A. Schuh, A. C. Lund, and T. G. Nieh, Acta Mater. **52**, 5879 (2004).